Catalysis Science & Technology

Accepted Manuscript

ROYAL SOCIETY OF CHEMISTRY

www.rsc.org/catalysis

Enhanced photocatalytic activity of Eu doped Bi_2S_3 nanoflowers for degradation of organic pollutants under visible light illumination

Arpita Sarkar,[a] Abhisek Brata Ghosh,[a] Namrata Saha,[a] Amit Kumar Dutta,[a] Divesh N. Srivastava,[b] Parimal Paul,[*b] and Bibhutosh Adhikary[*a]

[a]*Department of Chemistry, Indian Institute of Engineering Science and Technology, Shibpur, Howrah 711 103, West Bengal, India*

[b]*Department of Analytical Science, Central Salt and Marine Chemicals Research Institute, Gijubhai, Badheka Marg, Bhavnagar 364002, Gujarat, India*

Corresponding Author

*E-mail: bibhutoshadhikary@yahoo.in; Tel.: +91-033-2668-4561-64 ext: 512; Fax: +91-033-2668-2916.

Abstract: Europium (Eu) doped Bi_2S_3 nanoparticles (NPs) with different Eu contents were successfully synthesized by solvothermal decomposition of the precursor complexes $Bi(ACDA)_3$ and $[Eu(ACDA)_3 \cdot H_2O]$ [ACDA=2-aminocyclopentene-1-dithiocarboxylic acid] in ethylenediamine (EN). The precursors were characterized by usual techniques such as UV-Vis spectroscopy, FT-IR, CHN and TGA analyses. The prepared nanomaterials were characterized by XRD, EDX, SEM and TEM analyses. XRD results demonstrate that the particles were well crystallized. TEM images ascertain the NPs to be of flower-like structure consist of ultrathin nanoplates of average diameter of 9-10 nm. Photocatalytic efficiency of the Eu doped Bi_2S_3 NPs were evaluated by monitoring the degradation of methylene blue (MB) in aqueous solution under visible light. It was observed that the rate of photocatalytic degradation of MB increases with increase of dopant ion. In addition, the photocatalytic degradation of various toxic organic pollutants such as phenol, p-cresol, 4-chloro phenol, 4-tert-butyl phenol, 2,5-dimethyl phenol and 2,6-di-tert-butyl-p-cresol were carried out with doped NPs in visible light. Under identical condition, the degradation rate of 4-chloro phenol is higher than the corresponding phenol, p-cresol and 4-tert-butyl phenol. Finally, the mechanism of the degradation pathway for the phenol and substituted phenols is discussed.

Keywords: Eu doped Bi_2S_3 NPs, methylene blue, phenols, photocatalytic degradation pathway.

1. Introduction

Recently, a wide variety of organic pollutants are responsible for environmental and water pollution.[1] Among them, organic dyes, phenolic compounds and their derivatives are commonly used in various field and most of which are highly toxic and can remain in the environment in waste water for a long time.[2-4] These pollutants cause various environmental and serious health related issues in our society.[5,6] Although a variety of chemical, physical and biological methods are used for treatment of waste water but majority of these processes are expensive and not highly effective.[7-12] In this regard, uses of semiconducting nanomaterials for degradation of organic pollutants have many advantages over other methods because of their environmental friendliness, mild reaction condition and low concentration usage.[13,14] In particular, metal chalcogenides are finding increasing use as photocatalysts for degradation of toxic organic pollutants. In addition, the photodegradation of several toxic organic pollutants using TiO_2 as a photocatalyst has been extensively studied over past decade.[15-18] However, it is catalytically active only under UV irradiation because of its wide band gap energy, [19-22] which hinders its application in the visible region. Consequently, there is considerable demand for materials which are active in the visible region, since visible light is the main component in solar light and indoor illuminations.[23]

In this regard, sunlight-induced degradation of organic pollutants is one of the most attractive approaches for combating environmental pollution and wastewater treatment.[24] In order to improve the efficiency of utilizing solar energy, attention has been focused on designing visible-light driven photocatalysts. Over the last few decades, S-, N- and C doped TiO_2 photocatalysts have shown much promising as visible light induced photocatalysts.[25, 26] However, low quantum efficiency is a big problem for anion doped and co-doped TiO_2 – based photocatalysts. As a

result, non-titania–based catalysts which exhibit visible-light-driven catalytic activity have turned out to be promising alternartives.[27, 28]

Therefore, enormous efforts have been dedicated to search for highly efficient visible light driven photocatalysts in the past few years.[29-31]Moreover, a large number of reports have been focused on the synthesis of doped inorganic semiconducting chalcogenides for the degradation of organic pollutants through photocatalytic process.[32] Recently, Baibiao Huang and his group reported synthesis of $Bi_2O_2CO_3/Bi_2S_3$ and Bi_2S_3 nanocrystals/BiOCl heterojunctions and discussed their enhanced visible light-driven photocatalytic activity towards dye degradation.[33,34] In addition, rare-earth metal doped semiconductor has been a focus of numerous investigations because of its unique optical properties and promising applications due to contribution to the position of 4f electrons of rare-earth ions.[35,36] Furthermore, rare earth materials have been the subject of intensive interest as they are known for their ability to trap the electrons, which can effectively reduce the photogenerated electron-hole pairs. But pure rare-earth materials are very expensive; it is urgent to look for desirable host substance for the rare-earth materials or rare-earth host substance. In this respect, europium doped semiconductors have attracted much attention in photocatalytic process owing to its high photocatalytic activity for the degradation of organic contaminants.[37,38] Nevertheless, there have been no reports regarding the photocatalytic degradation of organic pollutants using Eu doped Bi_2S_3 NPs. Eu^{3+} can be doped in Bi_2S_3 moiety at ambient condition because of an ionic size closer to that of Bi^{3+}.[39] Therefore, doping of europium with Bi_2S_3 would be an efficient way to improve the photocatalytic activity.

In this study, we report a facile synthesis of Eu doped Bi_2S_3 NPs in different ratios through the decomposition of two single source precursors namely previously reported[40] Bi(III) dithiocarboxylate complex and newly synthesized Eu (III) dithiocarboxylate complex using

simple solvothermal technique. Furthermore, the doping percentage of Eu on Bi_2S_3 NPs is tuned to increase catalytic efficiency of the Bi_2S_3 NPs which were characterized by usual techniques. We demonstrated that the synthesized nanoparticles exhibit photocatalytic efficiency towards the degradation of methylene blue (MB), phenol and substituted phenols such as 4-chlorophenol, p-cresol, 4-tert-butyl phenol, 2,5-dimethyl phenol, 2,6-di-tert-butyl-p-cresol etc and the degradation kinetics using different ratios of Eu doped Bi_2S_3 NPs were studied thoroughly. Finally, the mechanism of the degradation pathway for the phenol and substituted phenols were studied which should provide important information about photocatalytic degradation pathway of other aromatic molecules.

2. Experimental

2.1. Chemicals and materials

All chemicals were of reagent grade and used without further purification. The ligand 2-aminocyclopentene-1-dithiocarboxylic acid (HACDA) was prepared according to the previously reported method.[41] Bismuth nitrate [$Bi(NO_3)_3 \cdot 5H_2O$], europium oxide (Eu_2O_3), ethylenediamine (EN), methylene blue (MB), phenol, 4-chloro phenol (4-CP), p-cresol, 4-tert-butyl phenol, 2,5-dimethyl phenol, 2,6-di-tert-butyl-p-cresol etc were purchased from Sigma-Aldrich. Millipore water, methanol, acetonitrile and diethyl ether were used as received.

2.2. Synthesis of precursor complexes

The precursor complex $Bi(ACDA)_3$ was synthesized by the reaction with [$Bi(NO_3)_3 \cdot 5H_2O$] and 2-aminocyclopentene-1-dithiocarboxylic acid (HACDA) which was reported previously.[40]

[$Eu(ACDA)_3 \cdot H_2O$] complex was synthesized using a stock solution of $Eu(NO_3)_3$ prepared by the digestion of Eu_2O_3 (175 mg, 0.5 mmol) in presence of conc.HNO_3. To a 10 mL clear

methanolic solution of $Eu(NO_3)_3$ (0.1 mmol), 15 mL HACDA (474 mg, 0.3 mmol) in methanol and triethylamine (301 mg, 0.3 mmol) mixture was added. A yellowish brown precipitate was immediately formed. After stirring for 15 min at room temperature, the product was filtered, washed in methanol and ether. Finally it was dried over calcium chloride. Yield- 450 mg (70 $^{o}/_{o}$).

Anal. ($C_{18}H_{26}EuN_3S_6O$): Found: C, 33.62; H, 4.59; N, 6.49. Calc. for $C_{18}H_{26}EuN_3S_6O$: C, 33.54; H, 4.50; N, 6.52%. FT-IR (λ_{max}, cm^{-1}): 3381 (m, br), 2928 (w), 1609 (s), 1466 (s), 1268 (w), 1037 (m), 790 (m). UV-Vis [$\lambda_{max}(CH_3CN)$/ nm (ε / M^{-1} cm^{-1})] 388 (9680).

2.3. Preparation of Eu doped Bi_2S_3 NPs

Eu doped Bi_2S_3 NPs in different ratios were prepared by solvothermal decomposition of the synthesized precursor complexes [$Bi(ACDA)_3$] and [$Eu(ACDA)_3 \cdot H_2O$] using nucleophilic solvent ethylenediamine (EN) in the following way**:**

The precursor complexes [$Bi(ACDA)_3$] (200 mg, 0.3 mmol) and [$Eu(ACDA)_3 \cdot H_2O$] (4 mg, 0.0062 mmol) were dissolved in 30 mL ethylenediamine and transferred into a Teflon-lined stainless steel autoclave. The temperature of the autoclave was maintained at 140° C for 5 h in a thermo-stated air oven. After that the black NPs, that deposited, were collected by centrifugation, washed several times with methanol and finally dried in air. The other two different ratios of Eu doped Bi_2S_3 NPs were prepared in a similar way by reacting the amount of [$Bi(ACDA)_3$] (200 mg, 0.3 mmol) with [$Eu(ACDA)_3 \cdot H_2O$] (6 mg, 0.0093 mmol) and [$Bi(ACDA)_3$] (200 mg, 0.3 mmol) with [$Eu(ACDA)_3 \cdot H_2O$] (10 mg, 0.0155 mmol), respectively.

2.4. Physical measurements

Elemental analyses (C, H and N) were performed using Perking-Elmer 2400 II analyzer. FTIR spectrum was recorded on JASCO FTIR-460 plus spectrophotometer using KBr disks. The electronic absorption spectra were recorded on a JASCO V-530 UV-Vis spectrometer. Thermo gravimetric analysis (TGA) was carried out using Perkin-Elmer USA Diamond-200 analyzer under nitrogen atmosphere with a heating rate of 10 ° C/min. Powder X-ray diffraction (XRD) were measured by the Philips PW 1140 parallel beam X-ray diffract meter using with Bragg-Bretano focusing geometry and mono chromatic Cu Kα radiation (λ = 1.540598 Å). Transmission electron microscopy (TEM) images were collected by using JEOL JEM-2100 microscope using an accelerating voltage of 200 kV. EDX analyses were carried out by using Hitachi S-3400 N (EDS, Horiba EMAX) instrument. The surface morphology of the materials was studied by Scanning electron microscopy (SEM) (JEOL-JSM-6360). The electro-spray ionization mass spectra (ESI-MS) were measured on a Micromass Qtof YA 263 mass spectrometer.

2.5. Photocatalytic Activity Measurements

The prepared Eu doped Bi_2S_3 nanoparticles were tested as photo-catalysts by the degradation of methylene blue (MB) and phenolic compounds in water. The experiments were carried out in a round bottom flask kept in a thermostated bath at 22° C. The light irradiation was carried out from a 200 W tungsten lamp (≥ 410 nm) and a 1 M solution of $NaNO_2$ was used as the UV cutoff filter.[42] The solutions of MB and phenolic compounds were prepared by dissolving it in Milli-Q Millipore water to obtain solutions of (2×10^{-5} M). The catalytic experiments were separately carried out with 40 mL aqueous solution using 10 mg of the synthesized catalyst. Before irradiation, the suspensions were magnetically stirred in the dark for 10 min to reach the

adsorption-desorption equilibrium. After a given interval of illumination, 3 mL of the aliquot was withdrawn from the solution mixture and centrifuged. The absorbances of the clear solutions were measured on a UV-Vis spectrophotometer.

3. Result and discussion

3.1. Synthesis

The precursor complex $Bi(ACDA)_3$ was synthesized according to the previously reported method.[40] The yellowish brown precursor complex $[Eu(ACDA)_3 \cdot H_2O]$ was synthesized by the reaction of $Eu(NO_3)_3$ with three equivalents of HACDA in methanol at room temperature (Scheme 1). The precursor complex is air stable and insoluble in water and common organic solvents, however, readily soluble in DMF and DMSO. The complex has been isolated in good yield and micro analytical data are consistent with the composition proposed.

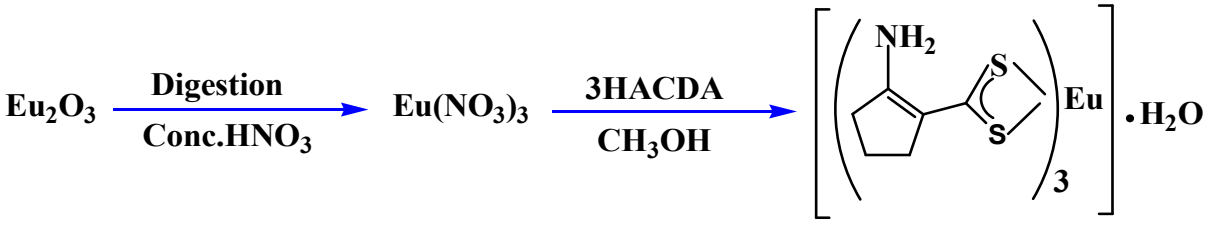

Scheme 1

The FTIR spectrum of the $[Eu(ACDA)_3 \cdot H_2O]$ (Fig. S1a) shows similar pattern compared to that of HACDA (Fig. S1 b) except a band at ~2500 cm^{-1} which appear in HACDA due to ν_{S-H} stretching frequency. The electronic absorption spectrum of the precursor complex (Fig.S2) shows one sharp absorption band at 388 nm and a shoulder at 322 nm, which may be due to the intra-ligand transition.

The Eu doped Bi_2S_3 NPs were prepared by simple solvothermal decomposition of the precursor complexes in EN at 140° C for 5 h (Scheme 2).

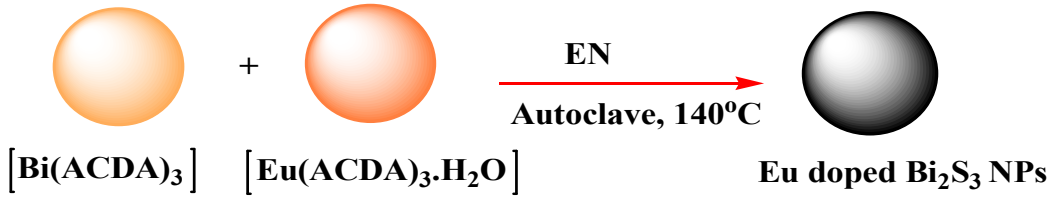

Scheme 2

3.2. Thermogravimetric analysis (TGA) of [Eu $(ACDA)_3 \cdot H_2O$] complex

The curve obtained from the thermogravimetric analysis (TGA) for [$Eu(ACDA)_3 \cdot H_2O$] complex is shown in Fig.1. The compound was found to decompose between 44 and 495°C through the following three steps, resulting in the formation of metal sulfide. At 397 °C the curve shows 27.99 $^{o}/_{o}$ residues, indicating the formation of EuS nanoparticle. The calculated weight percentage for the EuS residue is 28.41$^{o}/_{o}$, which is in good agreement with the value given by TGA. The first weight loss (2.836 %) between 68 and 118° C corresponds to the loss of one H_2O group (calc. wt $^{o}/_{o}$=2.797). The major weight loss (37.324 $^{o}/_{o}$) in the second step is observed in the temperature range of 118–226° C, which indicates the removal of one ACDA ($C_6H_8NS_2$) group and one C_5H_8N group (calc. wt% =37.269 $^{o}/_{o}$). The decomposition in the temperature range between 226–397 °C in the third step has been found to be 31 $^{o}/_{o}$, which is very close to the loss of remaining CS_2 and one C_6H_8NS group (calc. wt $^{o}/_{o}$=31.67 $^{o}/_{o}$). The weight loss curve becomes linear after 397° C, signifying no further changes in composition of the material. The possible chemical transformation equations for the thermal decomposition of [$Eu(ACDA)_3 \cdot H_2O$] are presented in the Scheme 3.

$$[Eu(C_6H_8NS_2)_3.H_2O] \xrightarrow{68\text{-}118^oC} [Eu(C_6H_8NS_2)_3] + H_2O \quad .....(1)$$

$$[Eu(C_6H_8NS_2)_3] \xrightarrow{118\text{-}226^oC} [Eu(C_6H_8NS_2)CS_2] + C_6H_8NS_2 + C_5H_8N \quad .....(2)$$

$$[Eu(C_6H_8NS_2)CS_2] \xrightarrow{226\text{-}397^oC} EuS + C_6H_8NS + CS_2 \quad .....(3)$$

Scheme 3

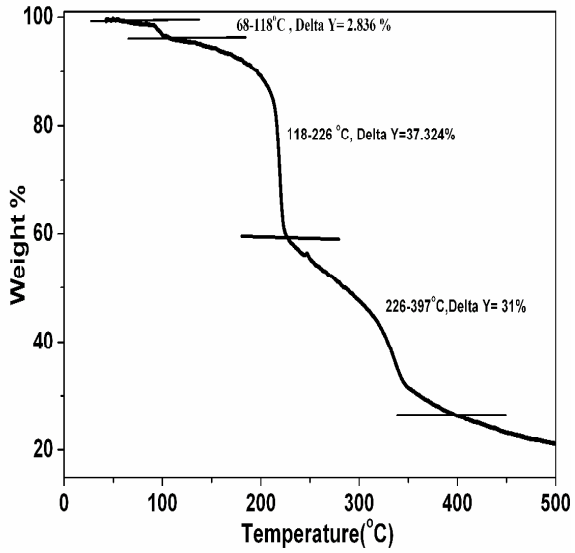

Fig.1

Fig.1 TGA curve of the $[Eu(ACDA)_3 \cdot H_2O]$.

3.3. Structural characterization of Eu doped Bi_2S_3 NPs

In order to confirm the formation of Eu doped Bi_2S_3 NPs and its crystalline phases, X-ray diffractgrams were recorded. Fig. 2A shows a comparison of the XRD patterns of the prepared samples of undoped Bi_2S_3 and Eu doped Bi_2S_3 in different ratios. As shown in the Figs. 2A(b), 2A(c) and 2A(d) the obtained XRD patterns show a set of four major peaks, centered at 2θ values of 19.95°, 26.09° , 30.13° and 45.05°, that are considerably broaden than the XRD patterns of the bulk pure Bi_2S_3 NPs [Fig. 2A(a)], although they have been made in a similar

method. Average crystal diameters for Eu doped Bi_2S_3 NPs were calculated using the Debye-Scherrer equation [$D= 0.9\lambda/(\beta cos\theta)$, where, D is the crystallite size, λ is the wave length of X-ray (1.540598 Å), β is the value of full width at half maximum and θ is the Bragg's angle] and found to be 9.5 nm.

The diffraction patterns of the bulk Bi_2S_3, presented in Fig.2A(a), match well with the standard diffraction data of the pure primitive orthorhombic phase of Bi_2S_3 (JCPDS No.170320). Unfortunately, the large peak broadening in case of Eu doped Bi_2S_3 NPs, due to the small crystal size make it difficult to obtain unambiguous crystal structure information from the XRD pattern of these doped Bi_2S_3 NPs. However, an accurate study combining HRTEM and SAED pattern will shed light on the crystalline structure of the NPs. A small shift (Fig. 2B) of the diffraction peaks are observed in case of the Eu doped Bi_2S_3 NPs, nevertheless this shift cannot be measured due to the low percentage of the dopant ion and the width of the diffraction peaks which is strongly broadened due to the small size of the crystallites. In addition, the EDX elemental analyses, as shown in Figs. S3, S4 and S5 confirmed that the nanocrystals were composed of Bi, Eu and S.

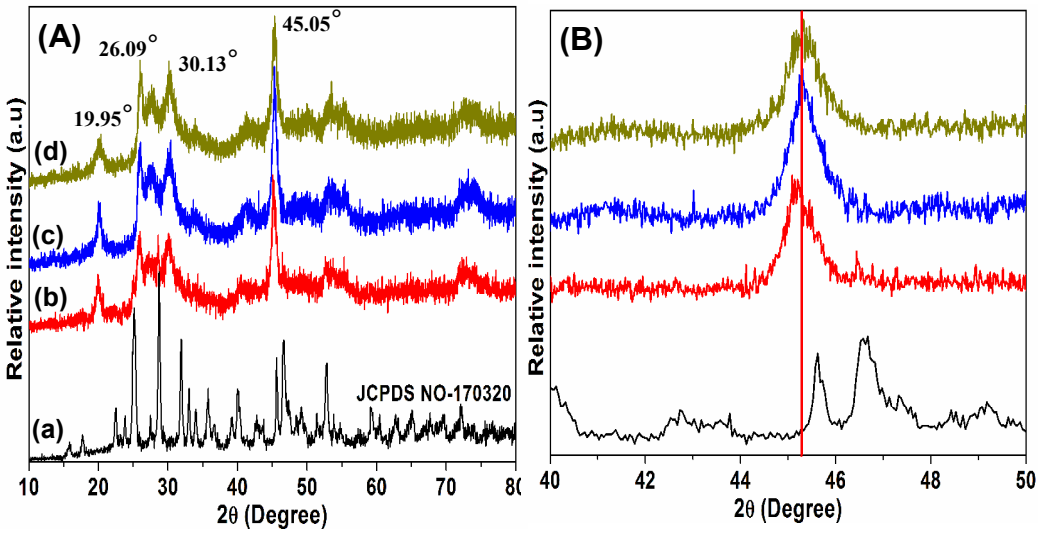

Fig. 2 (A) Powder X-ray diffractgram for (a) the pure Bi_2S_3 NPs (JCPDS No-170320), (b) 1.85 % Eu^{+3} doped Bi_2S_3NPs, (c) 2.32 % Eu^{+3} doped Bi_2S_3NPs, (d) 4.26 % Eu^{+3} doped Bi_2S_3NPs; (B) Zooming of XRD peaks centered at 45.05°.

The morphology of the as-formed Eu doped Bi_2S_3 NPs samples were examined by scanning electron microscopy and was shown in the Figs. S6(A) and (B), which revealed the formation of flower like aggregates with average diameter of 1.226 μm [Fig.S6(A)].

The above spherical flowerlike microstructures were also confirmed by TEM analysis and the images are shown in the Figs. S7, S8 and Fig.3. TEM images of undoped Bi_2S_3 NPs are also given in Fig.S9. Typical TEM images in those Figures show that the synthesized Eu doped Bi_2S_3 nanoparticles are composed of flower-like aggregates on a large scale, with average diameters of 1.276 μm [Fig.S7(A)]. It is interesting to note that with increasing the percentage of the dopant ion, size of the nanoflower moiety also increases (diameter for 1.85% Eu doped Bi_2S_3 is 1.269 μm, [Fig.S7(C)] for 2.32% Eu doped Bi_2S_3 is 1.505 μm [Fig. S8(C)] and for 4.26% Eu doped Bi_2S_3 is 1.841 μm (Fig. 3C). The average diameter obtained from TEM images are much higher than those of the XRD results, which was due to aggregation of the newly generated crystal nuclei. Detailed analysis of the NPs [Fig. S7(B)] revealed that each flower-like aggregate consist of ultrathin nanoplates which possess a relatively uniform thickness of 9-10 nm. Selected area electron diffraction (SAED) patterns of the 2.32% and 4.26% Eu doped Bi_2S_3 NPs exhibit sets of concentric rings that can be indexed to diffraction planes for (211), (120) (041) (231) [Fig.S8(D)] and (410) (301) (310) (200) respectively (Fig. 3D). The HRTEM image of Eu doped Bi_2S_3 NPs, displays clear image of lattice fringes of the prepared nanocrystals, indicating the good crystalline nature of the doped NPs.

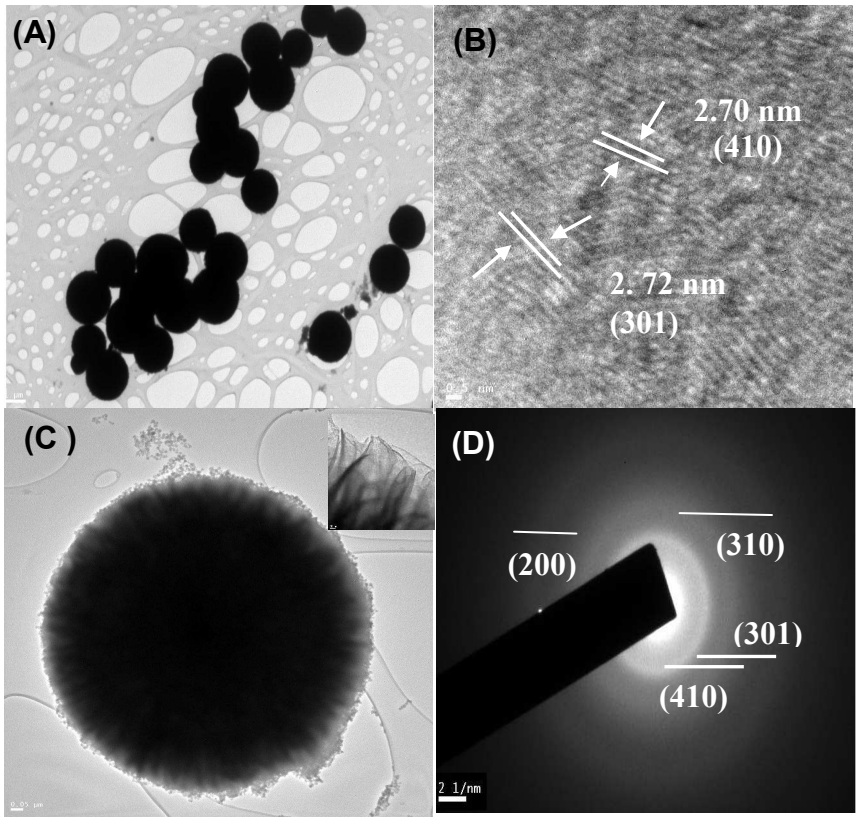

Fig. 3 TEM images of 4.26% Eu doped Bi_2S_3 NPs.

3.4. Optical properties

The optical property of Eu doped Bi_2S_3 prepared in different ratios were investigated by the UV-Vis absorption spectroscopy and the corresponding plots are shown in the Fig. S10 and Fig.4. The room temperature absorption spectra were recorded by dispersing the samples in methanol. The band gap energies (*E*g) of Eu doped Bi_2S_3 NPs were calculated from the band edge absorption using the Tauc's relation [$(\alpha h\upsilon)^{1/2}$ vs $h\upsilon$] (Fig. 4) and are found to be 2.55, 2.70 and 2.80 eV for Eu doped Bi_2S_3 NPs, where Eu=1.85, 2.32 and 4.26 $^{o}/_{o}$, respectively. The band gap energies are blue shifted with increasing the amount of the dopant ion compared to the bulk counterparts (for pure Bi_2S_3 band gap=1.7 eV) due to the quantum confinement effect. Further to

reveal the presence of Eu $^{+3}$ ion in the Bi_2S_3 moiety, photoluminescence spectra of pure Bi_2S_3 and Eu doped Bi_2S_3 (Eu=4.26%) were studied (Fig.S11).

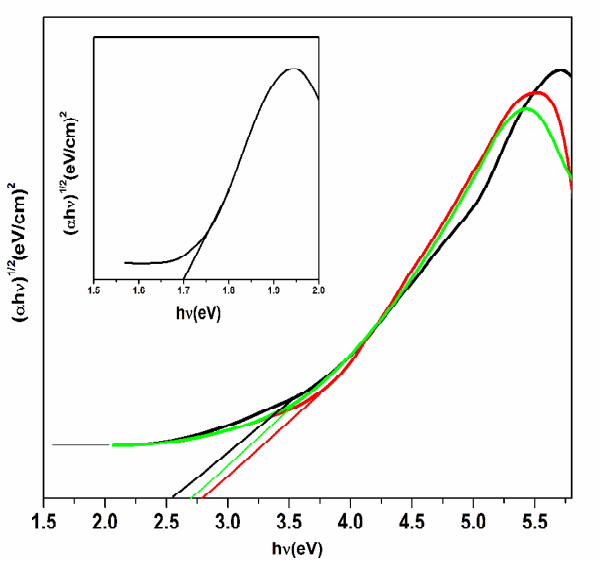

Fig. 4 Tauc's plot of Eu doped Bi_2S_3 NPs. Inset: Tauc's plot of undoped Bi_2S_3 NPs.

3.5. Photocatalytic degradation of MB

To investigate the potentiality of the prepared materials as photocatalyst, the catalytic performances of Eu doped Bi_2S_3 NPs were examined by the photodegradation of MB under the illumination of visible light as followed by spectrophotometric monitoring. We have chosen MB as representative organic dyestuff since it is resistance to biodegradation.

In order to establish relative performances of the synthesized three different Eu doped Bi_2S_3 NPs as photocatalyst with respect to pure Bi_2S_3 NPs and commercial WO_3 as standard samples, the following comparative studies were made using (2×10^{-5} M) MB solutions. 10 mg NPs were taken for doing all the experiments: (a) without catalyst in dark, (b) without catalyst in light, (c) with pure Bi_2S_3 NPs in light (d) with commercial WO_3 in light , (e) with Eu doped Bi_2S_3 NPs (

Eu= 1.85 %) in light, (f) with Eu doped Bi_2S_3 NPs (Eu= 2.32 %) in light and (g) with Eu doped Bi_2S_3 NPs (Eu= 4.26 %) in light (Fig.5A and Figs.S12, S13). Fig. 5B shows the comparative photocatalytic test under different conditions in terms of relative concentration (C_t/C_o) with irradiation time (t). The decomposition processes have been modeled as a pseudo first order reaction with the kinetic expression $ln(C_o/C_t) = kt$, where C_o represent the initial concentration of MB; C_t denotes the concentration at a given reaction time 't'. The comparative measurement show that, there is no such change in relative concentration of MB in absence of catalyst in dark and in light [Fig.5B (a) and (b)], indicates that degradation of MB is resistive in without any catalyst in dark and also in presence of light whereas, a negligible change is observed when it was kept in presence of pure Bi_2S_3 NPs [Fig.5B (c)] and in presence of commercial WO_3 [Fig. 5B(d)]. Remarkable changes can be observed in relative concentration of MB in presence of Eu doped Bi_2S_3 NPs and degradation up to 98 % is achieved using Eu doped Bi_2S_3 NPs (Eu= 4.26 %) under the light irradiation within 20 minutes. The degradation time has been found to be related to the percentage of Eu in the Bi_2S_3 NPs; greater the percentage of Eu in Bi_2S_3 NPs lesser will be the time of degradation. From the linear extrapolations (Fig. 5B inset), the reaction rate constants have been obtained and are given in Table S1.

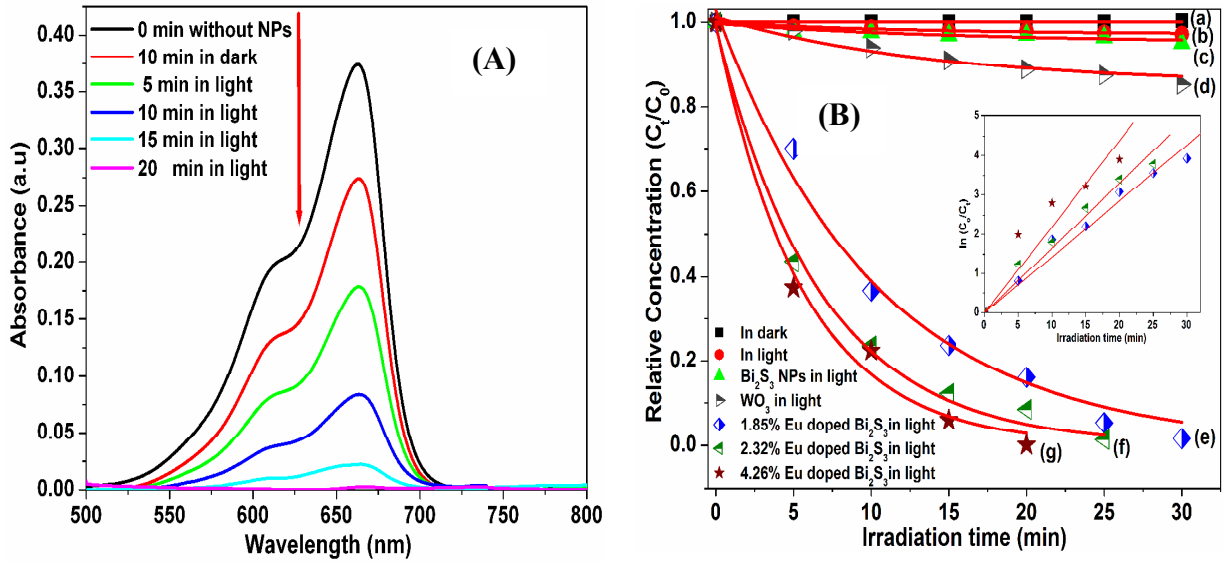

Fig. 5(A) Time dependent UV-Vis spectral change of MB solution (2×10^{-5} M) catalyzed by 10 mg Eu doped Bi_2S_3 NPs (Eu=4.26 %) (B) Photocatalytic degradation following pseudo first order kinetics of methelene blue under different conditions: (a) without catalyst in dark, (b) without catalyst in light, (c) pure Bi_2S_3 NPs in light, (d) commercial WO_3 in light , (e) Eu doped Bi_2S_3 NPs (Eu=1.85%), (f) Eu doped Bi_2S_3 NPs (Eu=2.32 %), (g) Eu doped Bi_2S_3 NPs (Eu=4.26 %). Inset: corresponding kinetic plot.

Therefore, these results indicate that Eu^{+3}dopant really could play an important role in the improvement of the photocatalytic activity of pure Bi_2S_3 NPs. This behavior can be attributed to the fact that the number of produced electrons and holes and their lifetimes are dependent on the kind and amount of dopant and the size of the semiconductor particles. When the band gap energy of a semiconductor is low, the lifetime of the produced electrons and holes in its surface is low, which decrease the photocatalytic activity. As the band gap energy of the Eu doped Bi_2S_3 NPs were higher than the pure Bi_2S_3, it can suppress the recombination of electron-hole pairs. It is cleared from the UV-Vis spectra that with increasing the amount of the dopant ion band gap energy of the synthesized NPs increase (2.55 eV to 2.80 eV). As a result, the Eu^{+3} dopant operate as an electron scavenger on the surface of Bi_2S_3 NPs, suppressing the recombination of electron-hole pairs and enhancing their lifetime, so the photocatalytic activity of photocatalyst is increased. In addition, we also studied the photocatalytic degradation of Rose bengal and Rhodamine B dyes in presence of visible light (Fig.S14, S15) .The reaction rate constants have been obtained from Fig.S16 and are given in Table S2.

The probable mechanism for the enhanced photocatalysis of Eu^{+3} doped Bi_2S_3 NPs is proposed as follows. Under visible light irradiation, electrons are excited from the valance band to the conduction band of Bi_2S_3, and holes (h^+) are produced. Eu^{+3} dopant in Bi_2S_3 can effectively

scavenge e^- and inhibit their recombination with holes (h^+). Due to the standard redox potentials of Eu^{+3}/Eu^{+2} and O_2/O_2^- [$E^0(Eu^{+3}/Eu^{+2}) = -0.36V$] and [$E^0(O_2/O_2^-) = -0.0338$ V], surface electrons could be trapped by the Eu^{+3} ion to form a reduced species Eu^{+2} ion, which then further oxidized back to Eu^{+3} by the adsorbed oxygen present in the system.[43] During these redox transformation, the species $O_2^{\bullet-}$ and ·OH will form and simultaneously, the adsorbed photogenerated holes oxidize water molecules or surface-bound hydroxide species to generate ·OH species. The mechanism is shown in equations 1-7.

$$Eu/Bi_2S_3 + \text{Visible light} \longrightarrow Eu/Bi_2S_3\,(e^- + h^+) \quad \text{.....1}$$

$$Eu^{+3} + e^- \longrightarrow Eu^{+2} \quad \text{(electron scavenging step)}\text{.....2}$$

$$O_{2ads} + e^- \longrightarrow O_2^{\bullet-} \quad \text{.....3}$$

$$O_2^{\bullet-} + Eu^{+3} \longrightarrow Eu^{+2} \quad \text{.....4}$$

$$Eu^{+2} + O_{2ads} \longrightarrow Eu^{+3} + O_2^{\bullet-}\text{(electron transferring step).....5}$$

$$h^+ + H_2O \longrightarrow {\cdot}OH + H^+ \quad \text{.....6}$$

$$h^+ + OH^- \longrightarrow {\cdot}OH \quad \text{.....7}$$

Furthermore, the stability of Eu doped Bi_2S_3 NPs were also examined by pursuing the MB degradation process with the Eu doped Bi_2S_3 NPs (Eu= 4.26 %) for three successive reactions. Slight decrease in catalytic activity (Fig.6) was observed after these successful reuses. Therefore, it is also concluded that the prepared Eu doped Bi_2S_3 NPs are stable enough for degradation reactions at normal condition.

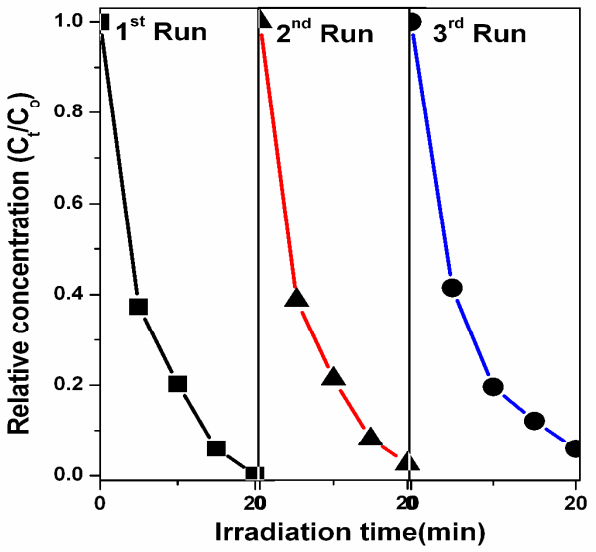

Fig. 6 Cyclic run for the catalytic decomposition of MB with Eu doped Bi_2S_3 NPs (Eu=4.26%).

3.6. Photocatalytic degradation of selected organic pollutants

In order to further investigate the enhanced photocatalytic activity of the prepared Eu doped Bi_2S_3 NPs, we have studied the photocatalytic degradation of more toxic compounds such as phenol, 4-chloro phenol, p-cresol and 4-tert-butyl phenol using only 4.26 $^{o}/_{o}$ Eu doped Bi_2S_3 NPs because its activity is maximum for MB degradation. The photocatalytic degradation experiments were performed using 40 mL of an aqueous solution of the appropriate pollutants (2×10^{-5} M) and 10 mg of 4.26 $^{o}/_{o}$ Eu doped Bi_2S_3 NPs as catalyst (Figs. S17, S18, S19 and Fig. 7A). From the $\ln(C_0/C_t)$ vs time (t) plot in Fig.7B inset, the highest rate is observed for the decomposition of 4-Chloro phenol followed by that of phenol, p-cresol and 4-tert-butyl phenol. The reaction rate constants have been obtained from the linear extrapolations plot (Fig. 7B inset) and are given in Table S3.

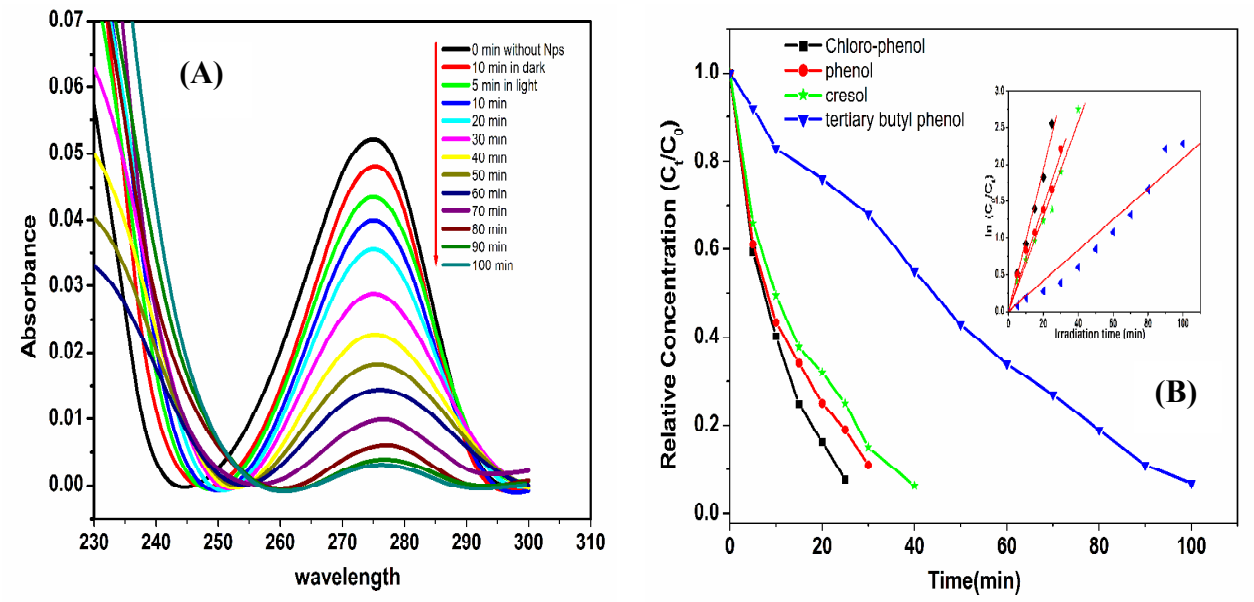

Fig. 7(A) Time dependent UV-Vis spectral change of 4-tert-butyl phenol solution (2×10^{-5} M) catalyzed by 10 mg Eu doped Bi_2S_3 NPs (Eu=4.26 %) (B) Relative Concentration (C_t/C_o) vs irradiation time (t) plot of different phenolic compounds catalyzed by 10 mg Eu doped Bi_2S_3 NPs under light irradiation. Inset: corresponding kinetic plot.

3.7. Mechanism of the degradation of phenol and substituted phenols (4-cp, cresol, 2,4,6-tertiary butyl phenol)

To investigate the mechanistic pathway in detail for the degradation of phenol and its different substituents, we have chosen various phenolic compounds mentioned in Table S4. Recently, very few groups have studied for the degradation of phenol, 4-CP, and p-cresol using TiO_2 as a photocatalyst.[15, 44, 45] They observed that the degradation process proceeds through the stepwise formation of various intermediates like catechol (CC), hydroquinone (HQ), hydroxyhydroquinone (HHQ) formed at the initial stage. These aromatic intermediates undergo

further photocatalytic oxidation to ring cleavage to yield carboxylic acids and aldehydes, which further degraded to CO_2 and H_2O.

In our study, the ESI-MS analysis of degraded solutions of these phenolic compounds show that the reaction pathway is not as similar as described above. The large number of intermediates which have been identified during the photocatalytic degradation of phenolic compounds indicated a complicated mechanism. These reactions proceed through the formation of a hydroxyphenyl radical (HPR) which in turn further converted to the dihydroxy-biphenyl (DHB) mentioned in Scheme 3 and 4. The formation of the various intermediates has been confirmed from mass spectra (Figs. S20, S21, S22, S23, S24, S25). The presence of hydroxyphenyl radical (HPR) as a short-lived radical intermediate has also been suggested in a recent study by electron paramagnetic resonance spin trapping detection during the direct photolysis of 4-CP.[46] All the bicyclic compounds will then be degraded under photocatalytic conditions into monocyclic compounds which further decomposed to carboxylic acid. It is interesting to note that the rate of degradation of 4-CP is higher than the rates of the other phenolic compounds. This phenomenon may be explained due to -I effect of Cl atom which stabilize the $H^{\cdot}$ radical formed by the photo degradation. But in case of other alkyl substituted phenols the electron donating ability of alkyl groups could not stabilize the aromatic ring and hence their rates are much slower than 4-CP.

The probable mechanism of degradation of Phenol and 4-CP are mentioned in Scheme 3 and Scheme 4. It is observed from mass analyses that p-cresol, 4-tert-butyl phenol, 2,5-dimethyl phenol and 2,6-di-tert-butyl -p-cresol are also follow the similar reaction pathway.

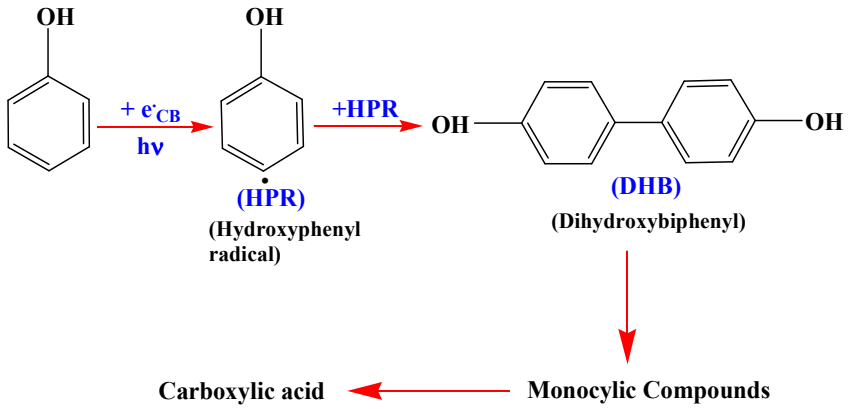

Scheme 3

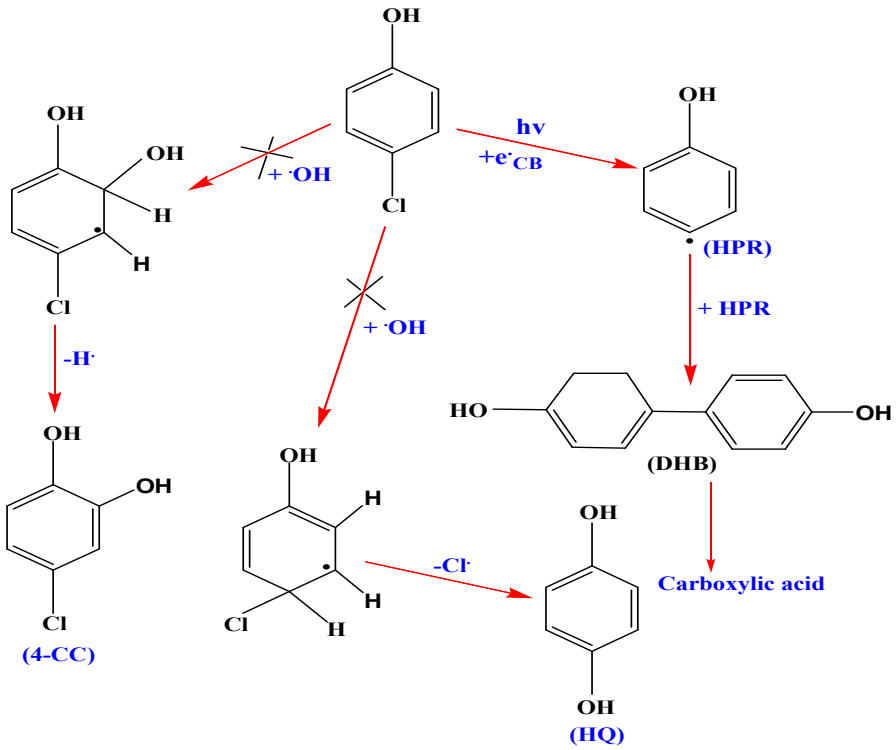

Scheme 4

4. Conclusion

In summary, a simple and efficient solvothermal method was applied for the synthesis of different ratios of Eu doped Bi_2S_3 nanoparticles as new visible light activated photocatalysts. The structural features of those materials have been studied by UV-Vis spectroscopy, XRD, EDX, SEM and TEM which supports the formation of Eu doped Bi_2S_3 NPs with an average diameter 9.5 nm. The results of XRD and EDX analyses confirmed that the doping of Eu ions into the Bi_2S_3 moiety did not change the crystal structure of pure Bi_2S_3 NPs. Optical characterization of the products revealed a blue shift in the band gap energies (2.55 eV to 2.80 eV) of the synthesized materials which is due to quantum confinement effect exerted by the nanocrystals. The synthesized nanoparticles showed excellent photo-sensitized photodegradation of MB and some typical organic pollutants such as phenol, 4-CP, p-cresol, 4-tert-butyl phenol under the illumination of visible light. This study of degradation of MB has shown that the synthesized Eu doped Bi_2S_3 NPs is more effective than commercial WO_3.

Kinetics of the degradation of MB and phenolic compounds were also investigated and found to follow the pseudo-first-order path. These photocatalysts are stable enough to be recycled several times. It was observed that with increase of the dopant ion, the photocatalytic activity of the NPs increases. This is due to the decrease in the particle size with increasing band gap energies with the incorporation of the dopant ion, which inhibit the electron-hole recombination and enhanced their life time. The mechanism of the degradation pathway for the phenol and substituted phenols were investigated. It was observed that hydroxyphenyl radical (HPR) was formed in each case, which is immediately further, converted to the dihydroxy-biphenyl (DHB) and formed a bicylic compound which will be then degraded under photocatalytic conditions into monocyclic compounds and finally to carboxylic acid. No detectable amounts of toxic impurities

such as catechol (CC) and hydroquinone (HQ) were present during the degradation of phenolic compounds with synthesized catalyst, which makes the Eu doped Bi_2S_3 NPs ecofriendly.

ACKNOWLEDGMENT

Authors are thankful to Prof. K. Nag, Department of Inorganic Chemistry, IACS, Kolkata, India, for helpful discussion. A. S is indebted to UGC (BSR), India, for his JRF [F. No.F.7-223/2009 (BSR)]. The authors also acknowledge CSIR (Scheme no. 01/2749/13/EMR-II) for funding and also MHRD (India) and UGC-SAP (India) for providing instrumental facilities to the Department of Chemistry, IIEST.

References

1 M. J. Benotti, R.A. Trenholm, B.J. Vanderford, J. C. Holady, B .D. Stanford and S. A. Snyder, *Environ. Sci. Technol*., 2009, **43**,597-603.

2 L.H. Kieth and W.A. Telliard, *Environ. Sci. Technol*.,1979, **13**, 416-423.

3 V. M. Brown, D.H.M. Jordan and B.A. Tiller, *Water Res*., 1967, **1**, 587-594.

4. A. Nuhoglu and B. Yakin, *Process of Biochemistry*, 2005, **40**, 233-239.

5 G.Tziotzios, M. Teliou, V. Kaltsouni, G. Lyberatos and D.V. Vayenas, *Biochem*. *Eng. J*., 2005, **26**, 65-71.

6. T.P.David, 3 rd ed.;Tata McGraw-Hill publishers:1978;pp 225-236.

7 S. Rengaraj, S.H. Moon , R. Sivablan , B. Arabind and V. Murugesan , *J. Hazard. Mater*., 2002 , **89**, 185-196.

8 A. Idris and K. Saed , *Global Nest: the int J.*, 2002, **4**, 139-144.

9 E. Miland, M. R. Smyth and C. O. Fagain, *J. Chem. Technol. Biotechnol.,* 1996 *,* **67***,* 227-236.

10 C. Comninellis and C. Pulgarin, *J. Appl. Electrochem.*, 1991, **21**, 703-708.

11 R. D. Yang and A.E. Humphrey, *Biotechnol. Bioeng*., 1975, **17**, 1211-1235.

12 A. F. Rozich, A.F. Gaudy and P.D.D. Adamo, *Water Res*., 1985, **19**, 481-490.

13. E. Forgas, T. Cserhati and G.Oros, *Environment International*, 2004, **30**, 953-971.

14 M.R. Hoffmann, S.T. Martin, W. Choi and D.W. Bahemann, *Chem. Rev*.,1995, **95**, 69-96.

15 K .Navaveni, G. Silvalingam, M. S. Hedge and G. Madras, *Environ. Sci. Technol*., 2004, **38**, 1600-1604.

16 A.L. Linsebrigler, G. Lu and J. T. Yates, *Chem. Rev*., 1995, **95**, 735-758.

17 W. Ren, Z. Ai, F. Jia, L. Zhang, X. Fan and Z. Zou, *Appl.Catal.B: Environ*., 2007, **69**,138-144.

18 Y. Chen and D.D.Dionysiou, *J. Mol. Catal. A: Chem*., 2005, **244**, 73-82.

19 X.B. Chen and S.S. Mao, *Chem. Rev*., 2007, **107**, 2891-2959.

20 D.W.Chen and A.K. Ray, *Appl. Catal. B: Environ*., 1999, **23**,143-157.

21 H. Gericher, *Top. Appl. Phys*., 1979, **31**, 115-172.

22 S. Kitano, N. Murakami, T. Ohno, Y. Mitani, Y. Nosaka, H. Asakura, K. Teramura, T. Tanaka, H. Tada, K. Hashimoto and H. Kominami*, J. Phys. Chem. C*, 2013,**117**, 11008-11016.

23 W. Zhao, C. Chen , X. Li, J. Zhao , H. Hidaka and N. Serpone, *J. Phys. Chem.B*, 2002, **106**, 5022-5028.

24 D.A.Keane, K.G.McGuigan, P.F.Ibanez, M.I.Polo-Lopez, J.A.Byme, P.S.M.Dunlop, K.O'Shea, D. D. Dionysiou and S. C. Pillai, *Catal. Sci. Technol*., 2014, **4**, 1211-1226.

25 S.U.M. Khan , M. Al-Shahry and W.B. Ingler, *Science,* 2002, **297**, 2243-2245.

26 S.In, A. Orlov, R. Berg, F. Garcia, S. P. Jimenez, M. S. Tikhov, D. S. Wright and R.M. Lambert, *J. Am. Chem. Soc*., 2007, **129**, 13790-13791.

27 M. Sun, D. Li, W. Li, Y. C hen , Z. Chen, Y. Xe and X. Fu, *J. Phys. Chem. C.*, 2008, **112**, 18076-18081.

28 C. Karunakaran and S. Senthilvelan, *Sol. Energy*, 2005, **79**, 505-512.

29 X. Zhou, S. Yao , Y. Long, Z. Wang and W. Li *, Mater. Lett*., 2015, **145**, 23-26.

30 E. Hu , X. Gao , A. Etogo , Y. Xie , Y. Zhong and Y. Hu, *J. Alloys Compd*., 2014, **611**, 335-340.

31 Y. Cui, Q. Jia, H. Li , J. Han, L. Zhu, S. Li, Y. Zou and J.Yang*, Appl. Surf. Sci.,* 2014, **290**, 233-239.

32 W. Wang, W. Zhu and H. Xu, *J. Phys. Chem. C*, 2008, **112**, 16754-16758.

33 H. Cheng, B. Huang, X. Qin, X. Zhang and Y. Dai, *Chem. Commun*., 2012, **48**, 97–99.

34 W. Wang, H. Cheng , B. Huang , X. Lin , X. Qin , X. Zhang and Y.Dai, *J. Colloid Interface Sci*.,2013, **402**, 34-39.

35 G. Xueyun, L. Zhengqing, Y. Dong, Z. Hongyang, L. Na, Z. Xinyu and D. Yaping ,*J. Mater. Chem. C*, 2015, DOI: 10.1039/c5tc00312a.

36 Y. Hasegawa, T. Adachi, A. Tanaka, M. Afzaal, P. O'Brien, T. Doi, Y. Hinatsu, K. Fujita, K. Tanaka and T. Kawaj , *J. Am. Chem. Soc*., 2008, **130**, 5710-5715.

37 T. Yu, Z. Lide and Z. Junxi, *Journal of Alloy and Compounds*, 2012, **537**, 24-28.

38 H. Shi, T. Zhang and H. Wang, *Journal of Rare Earth*, 2011, **29**,746-752.

39 M. Zhao, G. Li, L. Li, L. Yang and J. Zheng, *Cryst. Growth Des*., 2012, **12**, 3983-3991.

40 A. K. Dutta, S. K. Maji, K. Mitra, A. Sarkar ,N. Saha , A. B. Ghosh and B. Adhikary, *Sens. Actuators, B*., 2014, **192**, 578-585.

41 K. Nag and D.S. Joardar, *Inorg. Chim. Acta*, 1975, **14** ,133-141.

42 S. Jana and A. Mondal, *Appl. Mater. Interfaces*, 2014, **6**, 15832-15840.

43 P.V.Korake, A.N. Kadam and K.M.Garadkar, *Journal of Rare Earths*, 2014, **32**, 306-313.

44 J. Chen, L. Eberlein and C.H. Langford, *J. Photochem. Photobiol. A. Chem*., 2002, **148**,183-189.

45 C.S. Turchi and D.F. Oillis, *J.Catal*.,1989, **119**,483-496.

46 E.L. Kochany, J. Kochany and J.R. Bolton, *J. Photochem. Photobiol. A: Chem*., 1991, **62**, 229-240.

Graphical Abstract

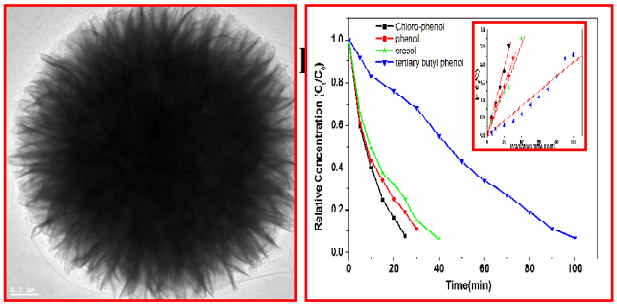

Eu doped Bi_2S_3 nanoflowers owing highly visible light driven photocatalytic activity towards degradation of organic pollutants